

Modeling solute transport and transient seepage in a laboratory beach under tidal influence

Michel C. Boufadel*, Yuqiang Xia¹, Hailong Li²

Center for Natural Resources Development and Protection (NRDP), Department of Civil and Environmental Engineering, Temple University, 1947 N. 12th Street, Philadelphia, PA 19122, USA

ARTICLE INFO

Article history:

Received 7 July 2010

Received in revised form

27 November 2010

Accepted 2 February 2011

Available online 26 February 2011

Keywords:

Solute transport

Transient seepage

Capillarity

MARUN

Laboratory beach

Tides

ABSTRACT

This paper explored numerical techniques to simulate the movement of an applied tracer plume in a laboratory beach subjected to tide. The MARUN model (Boufadel et al., 1999) was used. The movement of the tracer plume in the beach and the development of a transient seepage on the beach surface were modeled. By calibrating the results of the numerical model against the observed data, the laboratory beach was found to have two different zones: a top layer (thickness 9–17 cm) with a saturated hydraulic conductivity, K_0 , of 0.2 cm/s and a lower layer with a K_0 of 0.12 cm/s. The simulations revealed that the plume moved seaward during falling tides and downward during rising tides, which is consistent with previous studies. It was also observed that the plume developed a tail that extended in the landward direction, and a freshwater pool became entrapped between the main plume and its extended tail.

A sensitivity analysis was conducted to evaluate the effects of boundary conditions, seepage face development, capillarity, and dispersivity values. It was found that a Dirichlet boundary condition landward of the beach causes the plume of applied tracer to sink deeper into the beach in comparison with a Neumann boundary condition. The suppression of the seepage face by forcing the water table to match the tide level did not have great effects on beach hydrodynamics or on the movement of the tracer, which was probably due to the small slope of the beach (10%). However, seepage flow was around half of the seaward flow leaving the beach through the submerged face. Investigation on the capillarity through the van Genuchten parameter revealed that a decrease in the pore size of the beach greatly affects solute hydrodynamics; we noted that the effects on solute transport increase with depth. Thus, we conclude that using a saturated flow model for tidally influenced beaches should be discouraged, especially for fine textured media (i.e., small α or strong capillarity). The simulations also showed that dispersivity does not affect the travel time of the peak of solute concentration at a specific location but affects its magnitude.

© 2011 Elsevier Ltd. All rights reserved.

1. Introduction

The numerical simulation of groundwater hydrodynamics in coastal aquifers has rapidly evolved over the last three decades. Earlier studies were interested in locating the freshwater–salt-water interface and seawater intrusion (Pinder and Cooper, 1970; Shamir and Dagan, 1971; Frind, 1982), and for that reason they addressed the problem at the large scale (say tens to hundreds of

kilometers). Also, in situations where the aquifer was unconfined (i.e., the water surface is free to move up and down), the flow in unsaturated zone (i.e., above the water table) was not modeled directly but it was accounted for on the saturated flow using a specific yield coefficient (Bear, 1972; Huyakorn et al., 1987; Galeati et al., 1992). Baird et al. (1998) investigated numerically the effects of specific storage on the tidal signal propagation in shallow aquifer using a saturated flow model.

In the saturated flow models, the water table becomes an impermeable boundary for water flow and solute transport (i.e., no water flow will cross it), which is not realistic. In the variably saturated model, the water table is merely the location of points where the pressure is equal to zero, and water can traverse it downward and upward (Boufadel et al., 1999).

As interest in nearshore hydraulics emerged, simulation of the hydrodynamics (i.e., water flow and solute transport) at the beach

* Corresponding author. Tel.: +1 215 204 7871; fax: +1 215 204 4696.

E-mail addresses: boufadel@temple.edu (M.C. Boufadel), xiayqcug@gmail.com (Y. Xia), hailongli@cugb.edu.cn (H. Li).

¹ Present address: School of Environmental Studies, China University of Geosciences, Wuhan 430074, PR China.

² Present address: School of Water Resources and Environmental Science, China University of Geosciences-Beijing, Beijing 100083, PR China.

scale emerged in the last two decades to account for tidal hydraulic and for seaward boundary condition (e.g., Nielsen, 1990; Li et al., 1997; Turner et al., 1997; Park and Aral, 2008). Nielsen (1990) derived an analytical solution for tidal dynamics of the water table in sandy beaches that took into account the effect of the sloping beach surface. Turner et al. (1997) used the saturated flow numerical model MODFLOW to simulate the super-elevation of groundwater in a tidally influenced laboratory beach. Boufadel et al. (1998) reported water table variation with tide in a laboratory beach. They modeled the measurements using the MARUN (MARine UNSaturated) code (Boufadel et al., 1999). Applications of the modeling include quantification of the submarine groundwater discharge (e.g., Li et al., 1999; Destouni and Prieto, 2003; Robinson et al., 2007; Li et al., 2008) and the bioremediation of tidally influenced beaches (Venosa et al., 1996; Wrenn et al., 1997; Brovelli et al., 2007; Li et al., 2007; Robinson et al., 2009; Li and Boufadel, 2010; Xia et al., 2010).

Ataie-Ashtiani et al. (1999a,b) used the model SUTRA (Voss, 1984) to simulate the saltwater distribution in a tidally influenced aquifer. They also accounted for the development of the seepage face. Boufadel (2000) simulated low and high salinity experiments in a laboratory tank using the MARUN. They found that an inverted salinity distribution emerges whereby high salinity water occupies the intertidal zone and freshwater emanating from the landward side would form a tube that pinches out of the beach at low tide. Zhang et al. (2001) found that the saltwater wedge has a crucial impact on the circulation in the nearshore, and affects the position where the solutes injected landward are discharged.

Brovelli et al. (2007) numerically modeled laboratory experiments of a tidally influenced beach reported in Zhang et al. (2002). They accounted for the effect of tide and buoyancy and investigated the movement of applied plume of a conservative tracer. However, the software used for simulation was PHWAT a modified version of SEAWAT, based on MODFLOW, does not account for the unsaturated zone hydraulics (Langevin and Guo, 2006; Mao et al., 2006b; Brovelli et al., 2007).

Boufadel et al. (2006) conducted laboratory experiments to understand tidal effects on solute transport in tidally influenced beaches. They applied the tracer during a low tide onto the beach surface at the high tide line, and they monitored the plume movement throughout many tidal cycles. They found that tidal motion causes the plume to move downward during rising tides and seaward during falling tides. They also observed through the transparent side of the tank that a seepage face developed.

The main objective of this study was to numerically simulate the experiments conducted by Boufadel et al. (2006) using the most rigorous approach to better understand the overall behavior of the plume within the beach corporately considering the unsaturated zone hydraulics and seepage face. The numerical challenges are highlighted and remedial steps are taken. Sensitivity analyses are conducted to assess the role of model parameters on water flow and, more importantly, on solute transport within the beach.

2. Experimental setup

The laboratory experiment was conducted by Boufadel et al. (2006) in a laboratory beach 8 m long, 2 m high, and 0.6 m wide. The tank was made out of carbon steel, though one of the long walls of the tank was made out of Lexan (a type of reinforced Plexiglass) to allow visual observation into the tank. A screen was placed in the tank at 30 cm from the left wall (Fig. 1) to hold the sand and allow water passage. The water to the left of it represented the landward water table of the beach. The sand was placed in the tank at 10% slope from the elevation of 1.15 m on the screen to the elevation of 0.65 m at 5.0 m from the screen; the sand was then let to rest at its

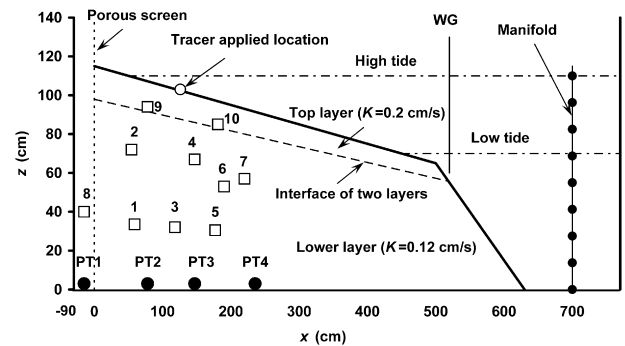


Fig. 1. Experimental setup showing concentration sensors (conductivity meters, CMs, squares), water piezometers (pressure transducers, PTs, filled circle), and tracer application location (circle). Wave Gage (WG) measures the water level at sea side (right-hand side of figure). The sensor locations are given in Table 1. This figure also shows two hydraulic properties zones: top layer with $K=0.2$ cm/s and lower layer with $K=0.12$ cm/s.

natural slope, this resulted in a total horizontal length of the beach of 6.3 m at the bottom (see Fig. 1).

The beach material consisted of coarse sand that had a median size of 1 mm and a particle size distribution varying from 0.8 mm to 1.2 mm. The porosity of the sand was 0.33. Boufadel et al. (1998) estimated a saturated hydraulic conductivity of 0.2 cm/s for this sand by conducting Bayesian estimation. They also obtained the values of van Genuchten (1980) parameters, i.e., $\alpha = 0.155$ cm⁻¹ and $n = 3.5$. The capillary fringe can be approximated as the inverse of α (about 6.45 cm).

The experiment started by filling the tank by tap water, whose background ion concentration was 0.15 g/L. The tide was simulated by pumping water in and out of the tank periodically through manifolds. The simulated tidal period was 37.5 min and the tide varied between 0.7 m and 1.1 m, resulting in an intertidal zone of 4.0 m. Two tidal cycles were completed prior to tracer application. Time zero was chosen at high tide level (see Fig. 2). When the water level reached the low tide level (at $t = 20$ min), the tidal cycle was stopped and a 100 L of a solution of NaCl at the concentration of 2.61 g/L was applied onto the beach surface for a duration of 24 min. The tidal cycle was then restarted. The application was centered at $x = 1.26$ m ($z = 1.03$ m) and extended 5 cm in both the seaward and landward directions, i.e., its imprint in the landward–seaward direction was 10 cm.

Four pressure transducers (piezometers, PTs) measuring the water pressure located at 3 cm above the bottom of the tank and 10 conductivity meter sensors measuring concentrations (CMs) were used for logging data (Fig. 1). The measurements were recorded every 30 s. The locations of PTs and CMs are given in Table 1. Note that the pressure sensor PT2 was not functioning (Boufadel et al., 2006).

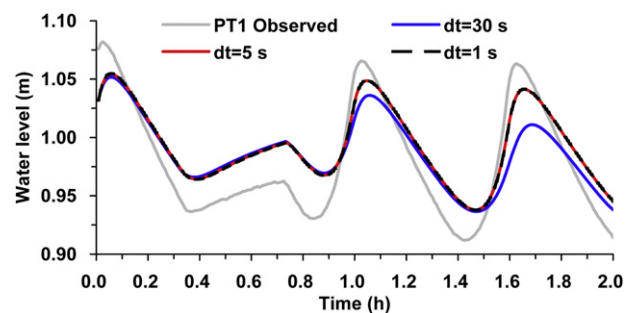


Fig. 2. Effect of time step (dt or Δt) on the simulated water level of PT1 (left of the screen in Fig. 1).

Table 1
Location of pressure transducers (PTs) and concentration sensors (CMs).

Sensor	x (cm)	z (cm)	y (cm)
PT1 ^a	-15	3	60
PT2	78	3	60
PT3	147	3	60
PT4	235.5	3	60
WG	520	NA	30
CM1	59	33.5	20
CM2	54.5	72	45
CM3	118	32	40
CM4	147	67	15
CM5	177	30.5	50
CM6	190	53	30
CM7	220	57	50
CM8 ^a	-15	40	30
CM9	78	94	15
CM10	181	85	10

Note: x is the horizontal distance from the screen (positive seaward), z is the elevation from the tank bottom, and y is the horizontal distance from the plexiglass wall (positive inward perpendicular to the plane of Fig. 1). "NA" denotes that data are not applicable.

^a Sensor is landward of the screen (see Fig. 1).

3. Numerical model

3.1. Governing equations

Numerical simulations were conducted using the MARUN model (Boufadel et al., 1999), which is a two-dimensional finite element code for density-dependent flow in variably saturated media. In the absence of source/sink terms, the equation for the conservation of the fluid mass (water plus solute) is written as:

$$\beta\phi\frac{\partial S}{\partial t} + \beta S_0 S \frac{\partial \psi}{\partial t} + \phi S \frac{\partial \beta}{\partial t} = \frac{\partial(\beta\delta K_x \frac{\partial \psi}{\partial x})}{\partial x} + \frac{\partial(\beta\delta K_z \frac{\partial \psi}{\partial z})}{\partial z} + \frac{\partial(\beta^2 \delta K_z)}{\partial z} \quad (1)$$

where t , x and z represent the time, the horizontal coordinate and the vertical coordinate, respectively. ϕ is the porosity [–], S is the water saturation ratio [–] (soil moisture divided by porosity), S_0 is the specific storage per unit fluid weight (L^{-1}), ψ is the pressure head [L]. K_x and K_z are the hydraulic conductivities [LT^{-1}], respectively. The left-hand side of Eq. (1) represents the variation of water mass with time and the right-hand side represents the variation in space of the horizontal and vertical flows. The term β represents a "state" equation:

$$\beta = \frac{\rho}{\rho_0} = 1 + \epsilon c \geq 1 \quad (2)$$

where ρ_0 is the freshwater density, ρ is the water density, and ϵ is a constant relating the concentration of salt (c) to the density of water. δ is the dynamic viscosity ratio defined as:

$$\delta = \frac{\mu_0}{\mu} = 1 - \xi c \quad (3)$$

where μ_0 and μ are freshwater dynamic viscosity and salt-dependent water dynamic viscosity [$ML^{-1}T^{-1}$], respectively. For $c > 0$, δ is less than 1.0, indicating that saltwater has higher resistance to water flow compared to freshwater.

The soil moisture and hydraulic conductivity are related by the van Genuchten (1980) model:

$$S_e = 1.0, \quad K_x = K_{x0}, \quad K_z = K_{z0}, \quad \psi \geq 0 \quad (4)$$

where K_{x0} and K_{z0} are the saturated horizontal and vertical freshwater hydraulic conductivity, respectively. For $\psi < 0$, the effective saturation ratio S_e is given by:

$$S_e = \frac{S - S_r}{1 - S_r} = \left[\frac{1}{1 + (\alpha|\psi|)^n} \right]^m \quad (5)$$

and K_x and K_z are given by:

$$K_i = K_{i0} \sqrt{S_e} \left[1 - \left(1 - S_e^{1/m} \right)^m \right]^2 \quad (6)$$

where $i = (x, z)$, $m = 1 - (1/n)$, S_r is the residual saturation ratio. Eq. (6) is based on the Mualem (1976) theory. The parameter α represents a characteristic pore size [L^{-1}], and higher α values imply a coarser material. The inverse of α provides an estimate of the capillary fringe (Boufadel et al., 1998). The term n represents the uniformity of the pores [–] and higher n values imply a more uniform pore size distribution (van Genuchten, 1980).

In the absence of source/sink terms the salt transport equation is given as:

$$\phi S \frac{\partial c}{\partial t} = \beta \nabla \cdot (\phi S D \cdot \nabla c) - \mathbf{q} \cdot \nabla c \quad (7)$$

where $\mathbf{q} = (q_x, q_z)$ is the Darcy flux vector given by:

$$\mathbf{q} = (q_x, q_z) = -K_i \delta \left(\frac{\partial \psi}{\partial x}, \frac{\partial \psi}{\partial z} + \beta \right), \quad i = (x, z) \quad (8)$$

The term D in Eq. (7) is the physical dispersion tensor:

$$\phi S D_{xx} = \alpha_L \frac{(q_x)^2}{\|\mathbf{q}\|} + \alpha_T \frac{(q_z)^2}{\|\mathbf{q}\|} + \phi S \tau D_f \quad (9a)$$

$$\phi S D_{zz} = \alpha_T \frac{(q_x)^2}{\|\mathbf{q}\|} + \alpha_L \frac{(q_z)^2}{\|\mathbf{q}\|} + \phi S \tau D_f \quad (9b)$$

$$\phi S D_{xz} = \phi S D_{zx} = (\alpha_L - \alpha_T) \frac{q_x q_z}{\|\mathbf{q}\|} \quad (9c)$$

where $\|\mathbf{q}\| = \sqrt{q_x^2 + q_z^2}$, α_L and α_T are the longitudinal and transverse dispersivities [L], respectively. D_f is the molecular diffusion coefficient [$L^2 T^{-1}$] and τ is the tortuosity of the pore space [–]. The first two terms on right hand side of Eqs. (9a) and (9b) represent mechanical dispersion of salt transport while the third term accounts for salt transport by molecular diffusion.

3.2. Boundary and initial conditions

On the sea side (beach surface), a seepage face was allowed to develop, which is an external boundary of the saturated zone where water leaves the soil and the pressure head ψ is uniformly zero. Since the height of the seepage face is generally not known *a priori* and is determined iteratively, the location of the seepage face is first estimated and then updated following the method introduced by Neuman (1973) and Pinder and Gray (1977). In other words, the location of the seepage face requires a check on the Darcy flux (q), which is computed usually by taking the derivatives (numerically) of the computed pressure head over each element. For example, at nodes where the pressure is negative ($\psi < 0$), a Neumann-type boundary is specified with the inwardly directed normal Darcy flux, i.e., $q = 0$. The final solution of numerical model will assign negative value for q (i.e., outward flow) at nodes where the pressure is prescribed as zero, and assign negative values for ψ at nodes where $q = 0$ (i.e., inward flow). More information can be found in Neuman (1973) and Cooley (1983). In the MARUN model, the Darcy fluxes are computed according to the method presented by Yeh (1981) because this method achieves continuity of the Darcy flux across element boundaries. The normal flux to the seepage face is computed subsequently. The simulation of the seepage face was

conducted according to the standard approach reported in Naba et al. (2002) and Li et al. (2008).

The no-flow and zero dispersion flux boundary conditions ($\partial\psi/\partial n = 0$ and $\partial c/\partial n = 0$) were used on the beach surface above the seepage face. Seaward of the seepage face, a Dirichlet boundary condition was set for water flow below the water level. The value of the pressure to use as Dirichlet boundary at each node was obtained from the observed data (H_{WG}) at the wave gauge (WG, Fig. 1), i.e.,

$$\psi(x, z) = H_{WG} - z(1 + \epsilon c_{sea}) \quad (10)$$

The simulation of the seaward concentration boundary condition of the submerged beach surface deserves a particular attention. Galeati et al. (1992) and Boufadel (2000) used the “outflowing boundary condition”; if the water is entering the domain, then a Dirichlet boundary was set for concentration which is equal to that in the seawater, i.e., $c(x, z) = c_{sea}$. If the solute is leaving the domain, then a Neumann boundary was assigned with a zero diffusive flux, i.e., $\partial c/\partial n = 0$. Therefore, the solute leaves the domain only by convection.

Park and Aral (2008) used the experimental results of Boufadel (2000) to investigate the effect of the boundary condition. They concluded that the “outflowing” boundary condition should not be used in situations where the seawater salinity is high and/or seaward groundwater flow is small. They proposed the usage of a Dirichlet boundary condition at the sea side regardless if the flow is entering or leaving the beach. The findings of Park and Aral (2008) were confirmed in the study by Abdollahi-Nasab et al. (2010) who reported experiments of saltwater flushing by freshwater under constant landward and seaward water heads. They modeled the results using the MARUN model and used a Dirichlet boundary condition on the sea side, as the outflowing boundary condition did not provide results that agreed with observations.

In this work, we used the outflowing boundary condition as the flow out of the beach was relatively high (in comparison with the work of Abdollahi-Nasab et al. (2010)) and because the concentration is relatively small (2.61 g/L).

In the tracer application segment (10 cm), a flux (Neumann) boundary condition was used whose value was obtained as follows. The flow rate covered the width (60 cm) of the tank and 10 cm in the landward–seaward direction. As the model is two-dimensional (a vertical slice), the flow per unit width of tank was assigned to the nodes in the 10 cm region. The horizontal spacing there was approximately 2 cm, and thus 5 nodes were made to be Neumann boundary nodes with the flow being equal to $2.13 \times 10^{-5} \text{ m}^2/\text{s}$. For the concentration, a Dirichlet boundary was assigned to these nodes, and the value was set at 2.61 g/L. That is to say, during the tracer application period P_{app} (24 min), the boundary conditions on the tracer application segment Γ_{app} were

$$\psi|_{(x,z) \in \Gamma_{app}} = 0, \quad \text{if } t \in P_{app} \quad (11a)$$

$$q|_{(x,z) \in \Gamma_{app}} = 2.13 \times 10^{-5} \text{ m}^2/\text{s}, \quad \text{if } t \in P_{app} \quad (11b)$$

$$c|_{(x,z) \in \Gamma_{app}} = 2.76 \text{ g/L}, \quad \text{if } t \in P_{app} \quad (11c)$$

$$c_{tracer}|_{(x,z) \in \Gamma_{app}} = 2.61 \text{ g/L}, \quad \text{if } t \in P_{app} \quad (11d)$$

Before and after the tracer application period, the natural infiltration boundary conditions in Eq. (11) were replaced by the no-flow and zero dispersion flux Neumann boundary conditions ($\partial\psi/\partial n = 0$ and $\partial c/\partial n = 0$).

The left boundary of the domain (representing the steel wall) was modeled as a Neumann boundary for water flow and solute transport, i.e., $\partial\psi/\partial n = 0$ and $\partial c/\partial n = 0$. The condition on water

Table 2
Model parameter values used in the numerical simulation.

Symbol	Definition	Unit	Value
α	Sand capillary fringe parameter of the van Genuchten (1980) model	1/m	25
n	Sand grain size distribution parameter of the van Genuchten (1980) model	–	3.5
K_0	Saturated freshwater hydraulic conductivity	m/s	2×10^{-3} (Top layer) 1.2×10^{-3} (Lower layer)
α_L	Longitudinal dispersivity	m	0.02
α_T	Transverse dispersivity	m	0.002
S_0	Specific storage	1/m	0.0
S_r	Residual soil saturation	–	0.01
ϕ	Porosity	–	0.33
CONVP	The convergence criterion of pressure head in the Picard iterative scheme of MARUN code	m	10^{-5}
τD_m	Product of tortuosity and diffusion coefficient	m^2/s	10^{-9}

ensures that no water crosses the steel wall. For the solute, this indicates that no solute leaves or enters the domain by diffusion, i.e., the solute flux would be only resulted from convection. In addition, a no-flow boundary condition was set in the equation to guarantee no solute flux entering or leaving the domain.

The model was run without tracer application for two tidal cycles and the water table at the last high tide was used as initial condition for the tracer application experiment. This replicates the way the experiment was conducted.

3.3. Numerical implementation

The space between the beach screen and the left wall (Fig. 1) was also modeled and assumed to be a very porous material with saturated hydraulic conductivity of 10 cm/s. Because the “porosity” of water body is 1.0 and that of the sand in the experiment was 0.33, the space behind the screen was considered to be filled with sand instead of water and that was assumed to be $0.3 \text{ m} \times 1.0/0.33 = 0.9 \text{ m}$ long, so that the simulated total water volume is equal to the observed one if the water levels were the same. The dispersivities in that region were set at 100 times their counterparts in the beach to account for high mixing in the open water. Fortunately, the values of dispersivities in that region were not critical as little tracer applied on the beach surface arrived at that region, and it was toward the end of the experiment. The calibrated values of model parameters based on MARUN simulations are summarized in Table 2.

The domain was discretized resulting in a total number of 31,320 triangular elements and 15,982 nodes. The horizontal and vertical spacing between nodes was 2.5 cm and 2 cm at the most landward position, and it decreased to 2.0 cm and 1.1 cm at the most seaward location, respectively. The simulation of 10.6 h of real time was conducted.

The main goal was to match as close as possible the observed data from all water level and concentration sensors, and we elected to do so by visually comparing simulated results to observed data. An automated calibration (e.g., Carrera and Neuman, 1986a,b; Boufadel et al., 1998) was not considered, as the simulation time of the experiment was too high.

4. Results

4.1. Effects of the time step

Fig. 2 shows the effects of the time step (Δt) on the accuracy of the solution at PT1: $\Delta t = 30 \text{ s}$ was not accurate whereas $\Delta t = 5.0 \text{ s}$

and $\Delta t = 1.0$ s had the same accuracy. Thus, we adopted the $\Delta t = 5.0$ s. The observed data were recorded every 30 s but the time interval was 5 s, hence linear interpolation was used to obtain observed data at 5 s intervals. The number of time steps was 7640 resulting in approximately 24 h of simulation time due to, among other, the simulation of the seepage face.

4.2. Density of the applied solution

The applied solution had a concentration of approximately 2.76 g/L (its density contrast to the tank water was 2.61 g/L). One of the major concerns was to investigate whether the density of the applied solution affected water flow. For this reason, a simulation where the effect of salinity on density was accounted for was compared to a simulation where the solute was used as a tracer, i.e., $\epsilon = 0$ in Eq. (2). The difference was negligible which is probably due to the high pore water velocity due to tide (a variation of 0.40 m in the tide within approximately 30 min). The comparison is not shown in this paper for brevity. Therefore, it was concluded that the density of the applied solution did not play a role in the transport in the tank. This means that the solute acted as an inert tracer, as intended by design.

4.3. Hydrodynamic properties of the beach

When the beach was assumed homogeneous, there was not a value for the saturated hydraulic conductivity that ensured matching the observed data, especially the concentration. This included various anisotropy ratios up to $K_{x0}/K_{z0} = 10$. For this reason, we explored piecewise homogeneity within the sand, and we found that the beach needed to be treated as consisting of two zones: a top layer with $K_{x0} = K_{z0} = 0.2$ cm/s and its thickness changed from 17.0 cm at $x = 0$ m to 9.0 cm at $x = 5$ m, and a lower layer with $K_{x0} = K_{z0} = 0.12$ cm/s. This is because of two facts: (1) the sand was compacted in place using a concrete vibrator (a 40 cm long, 1 inch wand), which tended to engender more compaction deep into the beach. At the beach surface, the vibrator simply redistributed the sand as there was no overburden weight to compact it, and (2) experiments were conducted where the beach was subjected to tides and waves which tended to mobilize the sand of the top portion of the beach. It is important to note that the 9–17 cm transition was obtained by trial and error and that the transition between layers is probably more diffuse. However, the adoption of only two layers appeared to be sufficient to capture the overall behavior of the applied plume.

The longitudinal dispersivity (α_L) was found to be 2 cm throughout the domain, and the ratio of longitudinal to transverse dispersivities α_T/α_L was set at 0.1. The value of α_T/α_L was assigned with 0.33 by Boufadel (2000) and 0.2 by Kim et al. (2004) for sandy beaches. The effect of dispersivity is further discussed in Section 5.

The water level results are given in Fig. 3. At the pressure transducer (PT1), the simulated water level responded slower to the tide than the observed one. The peaks were lower and the troughs were higher. Increasing the hydraulic conductivity value of the top layer made the match good, but the match became much poorer at other sensors, especially in terms of solute transport. It is possible that three-dimensional pathways of high hydraulic conductivity existed within the sand, and caused such a fast response of the observed data at PT1. In other words, as the simulation was based on two-dimensional representation of the beach, the saturated hydraulic conductivity value represents an average across the tank. A high value at one location might not influence the average considerably, but it would be sufficient to carry water back and forth between the “sea” side and the landward side of the beach. Such pathways would, in reality, result in

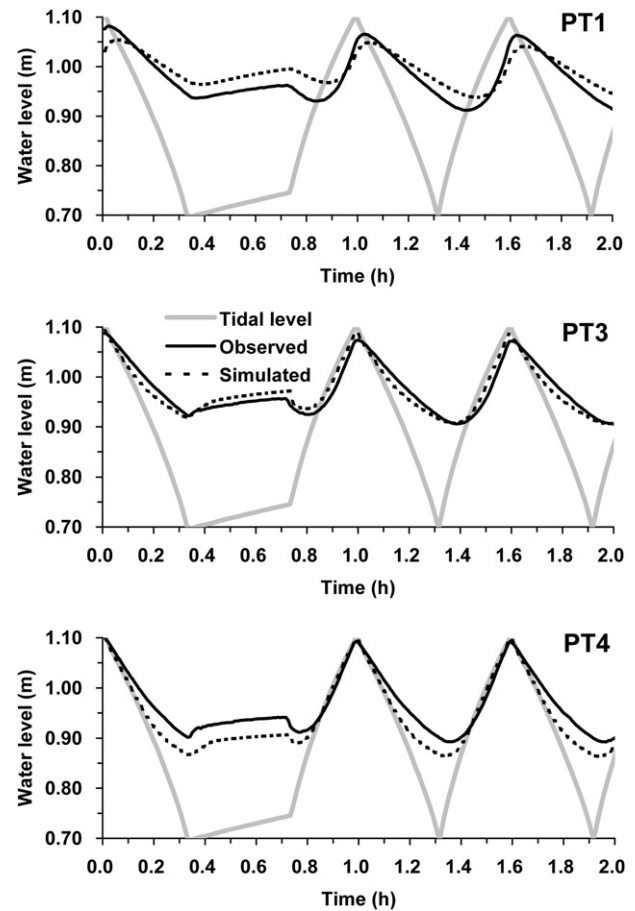


Fig. 3. Variations of water level at different piezometers. Note that simulated results reproduced the rise of water level during the application of tracer ($20 \text{ min} \leq t \leq 44 \text{ min}$).

faster response of the water level at PT1 in comparison with the exchange based on the two-dimensional model, which does not account for these pathways. Accounting for such pathways empirically would cause us to deviate from the rigor that we seek in this simulation, and from its main goal, which is to better understand the hydrodynamics at the beach scale.

Fig. 3 shows that the simulated water level at PT3 located beneath the tracer application area (Fig. 1) followed closely the observed data. Matching this sensor is important as the sensor should be less affected by the boundary effects than PT1 and PT4, and therefore more representative of the water table within the beach. For PT4 (the most seaward piezometer, Fig. 1), the simulated water level dropped faster than the observed one, and the maximum difference was about 3.0 cm. Fig. 3 shows that the rise of the water table due to the application of the tracer solution was captured by the model on all pressure transducers, though the match at PT3 was best.

Fig. 4 presents concentration results from all sensors (CMs). The agreement between the simulated and observed data was better for sensors seaward of the application area. For CM10, the simulated and observed data overlapped well for both peak time and peak value. At CM9, the peak time was closely matched, but the peak value was underpredicted. At sensor CM4, the closest to the application area, the simulated data followed the observed data with an overprediction of the peak value. A similar behavior was observed at CM6. The simulated results rose and dropped faster than observed data at CM7. The only concentration sensor placed landward of screen was CM8, its observed data and simulated

results showed that this sensor was reading the background concentration at all times (Fig. 4).

Three major factors affected the agreement between the simulated and observed results. First, the sensors (CMs) were encased in

screened plexiglass boxes whose dimensions were 10 cm × 10 cm × 10 cm. These boxes were used because the CMs do not work when they are in direct contact with sand. Thus, the observed value represents an average of a volume that is most likely

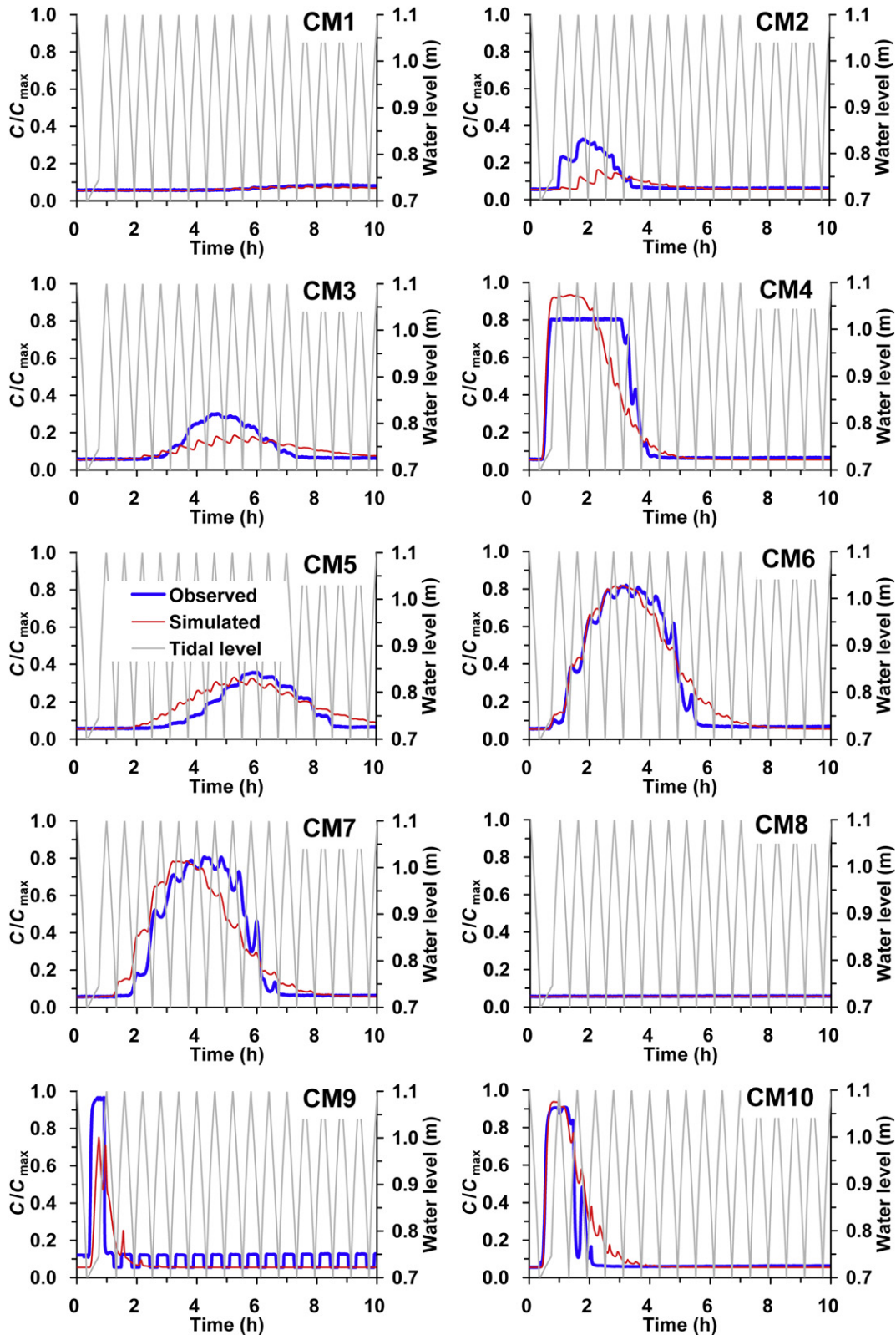


Fig. 4. Observed and simulated concentrations normalized by dividing by $C_{max} = 2.76$ g/L at all sensors.

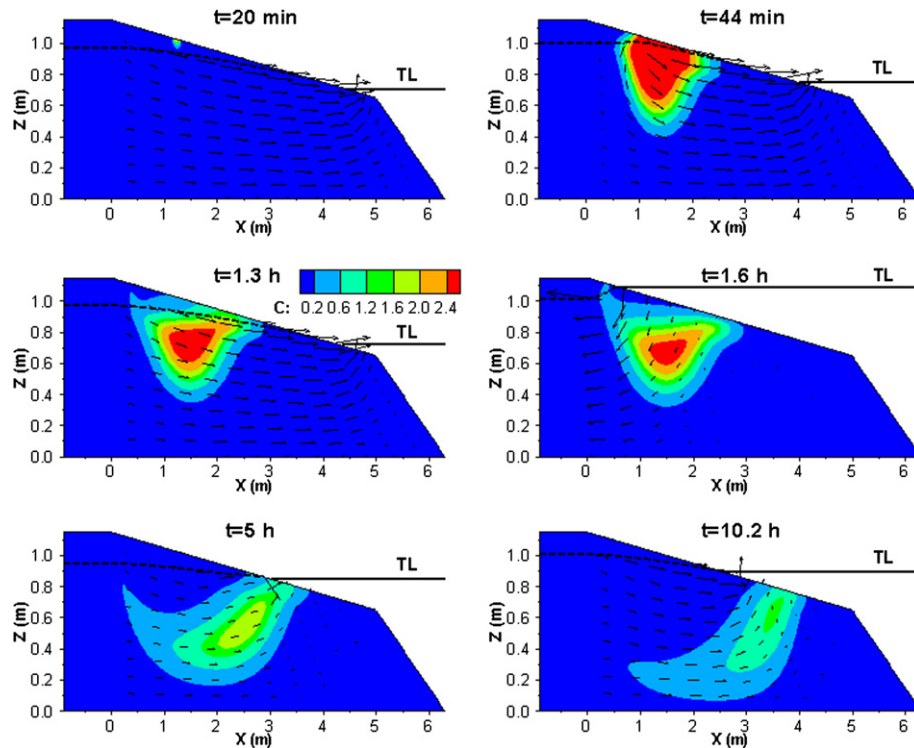


Fig. 5. Concentration (in g/L) contours at different times along with velocity vectors (arrows) and water table (dashed line). A freshwater pool existed close to surface between the center of the concentration plume and its extended tail ($t = 1.6$ h, 5 h, and 10.2 h). The solid line represents the tidal level (TL). This figure suggests that even under a no-flow landward boundary condition the tracer plume still moved seaward.

well mixed (due to the hollow volume within the plexiglass boxes), while the modeling results represent point values. This could explain, for example, the more dynamic behavior of the simulated results at CM7 in comparison with the observed ones: the point value would rise and drop faster than the average. Second, the simulated beach domain represented an idealized scenario. In reality, the beach surface changed with time due to the erosion during tide, especially at $x = 5.0$ m where the beach slope changed (see Fig. 1), and there was no way that we could account for that in the model without introducing a large degree of subjectivity. In addition, it is possible that local heterogeneity (say at 10–30 cm scale) existed in the tank, which would create different pathways (including three-dimensional pathways) that are not accounted for in the piecewise homogeneous model. Third, due to the relatively sharp edge of the plume (α_L is only 2.0 cm), the concentration varies greatly with space. Thus, the concentration reached the maximum at one location and was less than 10% of the maximum at 10 cm from that location (in any direction).

Fig. 5 reports the distribution of the tracer plume at various times. From $t = 20$ min to 40 min, the tracer application occurred and the water level was at low tide, causing the velocity vectors near the application area to be relatively large. A seepage face developed during application and was simulated herein, it can be noted at the end of the application ($t = 44$ min). The simulated concentration reached its maximum at this time as well. At $t = 44$ min, a sudden narrowing of the plume (going downward) was observed around $x = 2.1$ m, and $z = 0.8$ m, which is due to the fact that plume entered the lower layer whose hydraulic conductivity is lower than the upper layer (see Fig. 1). At $t = 1.3$ h, the plume was discharging to the sea during low tide. A tail of the plume is noted close to the application area. It spread landward and connected to the surface as the tide rose at $t = 1.6$ h and pushed the plume landward. Using the terminology of Brovelli et al. (2007),

a “pool” of clean water (referred as to “freshwater pool” hereafter) became entrapped between the main plume and its extended tail (e.g., $t = 5$ h). As the plume moved more seaward and downward with each tidal cycle, the size of the clean water pool increased (see $t = 5.0$ h). Going from $t = 5.0$ h to $t = 10.2$ h, the pool occupies the whole area landward of the plume, which indicates that the sea is filling the beach landward of the low tide line ($x = 4.5$ m, $z = 0.7$ m). Otherwise, the distribution of the plume would not change and only its concentration would decrease due to dilution by the tide.

In general, the plume got closer to the beach surface and diluted with tidal fluctuations. It remained connected visually to the low tide line while it rotated counterclockwise. It is as if the low tide line was a “hinge” for the plume to rotate around. This suggests that the landward flow near the low tide line (during rising tides) is negligible and that the seaward flow during low tide causes the plume to funnel upward toward the low tide line. The funneling is enhanced by the fact that the subtidal zone (zone of the beach seaward of the low tide line) is essentially stagnant, which is due to the hydrostatic boundary condition at sea. Since the tide represents a uniform head in the sea side (though variable in time), water propagating seaward takes the shortest path, which is upward through the low tide line, rather than moving seaward and facing more resistance within the sand. This was noted in our previous studies (Boufadel, 2000; Li et al., 2008; Li and Boufadel, 2010). At latter times, one sees that the plume moved about 0.3 m downward and about 2.0 m seaward.

Fig. 6 shows how the mass in the system changed with time. Summation of mass leaving the system and the mass remaining in the system at each time step provided the total mass (the initial mass in the experiment was found after tracer application, due to background the available mass in the domain was almost 160 g and the applied mass was 260 g which made the total mass 420 g). Thus, the model was accurately able to capture the applied mass. The mass

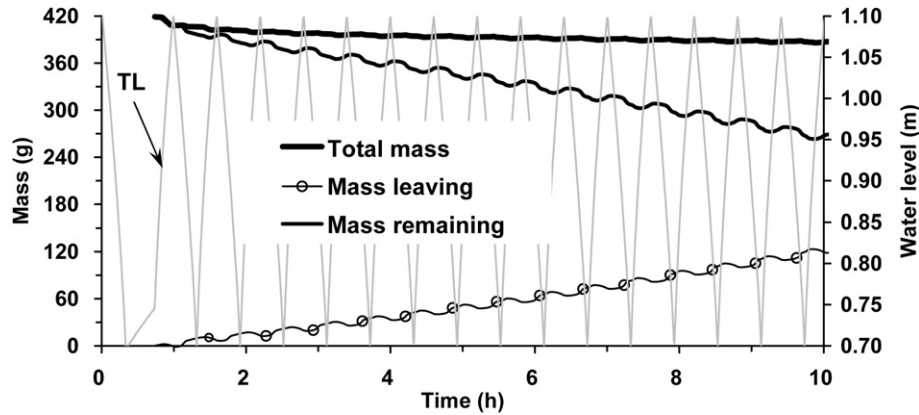


Fig. 6. Change of cumulative masses leaving and remaining in the domain along with the total mass with time. The total mass (or initial mass) in the system slightly decreases with time due to numerical error.

leaving the domain plus the mass remaining in the domain at each time should be equal to the total mass, but as time goes on, a slight error (<5%) was observed in the model (top line in Fig. 6 is not exactly horizontal). The difference is due to numerical error, and we believe mostly in accounting for the mass leaving, as the velocity gradients become too high, and it is possible that our mesh is not fine enough to capture the whole mass. Nevertheless, the error in mass balance is 5% which is still reasonable considering the highly dynamic nature of the system (tidal range is 40 cm) in the presence of a transient seepage face. Fig. 6 also shows that the mass remaining in the beach decreased almost linearly with time after the application. The fluctuations, which were due to tide, seem to be simply superimposed on the general trend. Thus, the behavior of the mass seems to be independent of its value, but rather controlled by convection–dispersion mechanisms that assured almost constant delivery of the tracer to the sea. This is probably due to the orientation of the plume which caused its discharge to the sea to be dependent on the zone near the low tide line. It is as if beach hydraulics resulted in a “bottle neck” effects whereby the discharge of the tracer mass to the sea depends on the available “opening” to the sea rather than on the total mass of tracer in the beach. To our knowledge, this local control was not noted before.

Fig. 7 reports the variations of the flow occurring through the seepage face (seepage flow), that occurring through the submerged surface (submerged flow), and the sum of them (total flow) on the beach surface. When the tide was falling, the submerged flow rise its

peak almost immediately and flattened out until the rising tide reached the elevation 0.95 m. The seepage flow increased gradually and its peak occurred exactly at low tide and then decreased suddenly, and continued to decrease until the rising tide reached the elevation 0.95 m. This elevation (0.95 m) corresponds to the lowest elevation of the water level at PT1. Therefore, it seems that in spite of the local controls on water flow out of the beach, the overall hydraulic gradient played an important role. During the application of the tracer ($20 \text{ min} \leq t \leq 44 \text{ min}$) the peak value of the seepage flow was higher than at latter times, but the peak of the submerged flow remained the same. In this case, the seepage flow accounted for ~59% of the total flow, while it became 34% of the total flow at latter times.

5. Sensitivity analysis

Four different scenarios were investigated to assess the sensitivity of the beach hydrodynamics to the conceptualization of the model and the parameters' values. The above-discussed simulation is referred to as the “base case”.

5.1. Landward boundary conditions

There are situations where the modeler cannot ascertain whether a Neumann or a Dirichlet boundary condition should be used at the landward side of the beach. A Neumann boundary condition should be used if the elevation of the landward water table of the beach is due

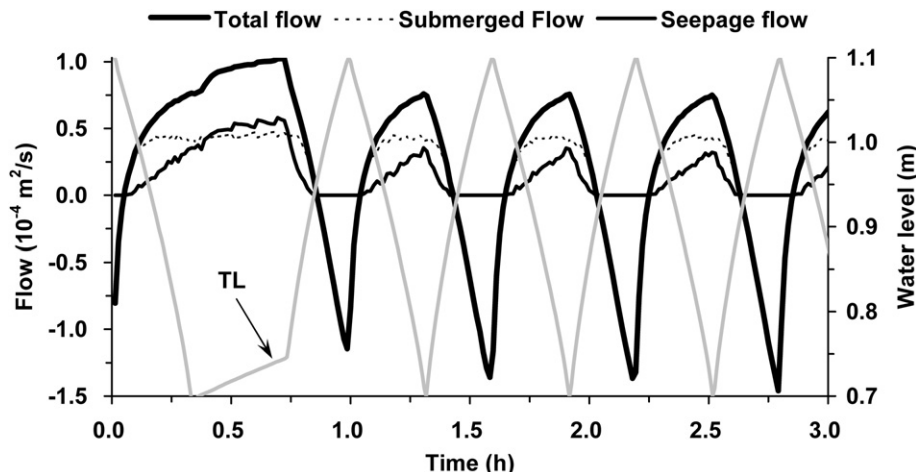


Fig. 7. Time series of seepage flow, submerged flow, and total flow (the sum of seepage flow and submerged flow). Also shown is the tide level (TL), read on the right axis.

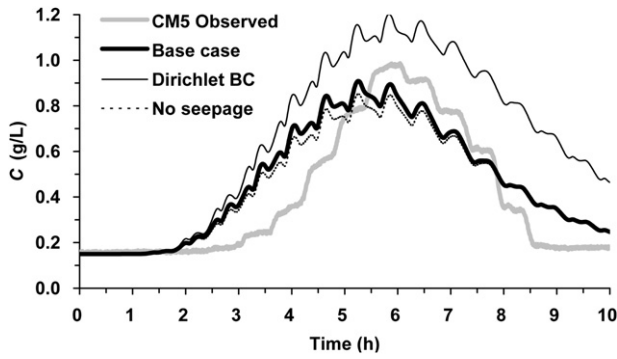


Fig. 8. Variation of the simulated concentration (in g/L) at CM5 for various scenarios. Note that a Dirichlet boundary condition (Dirichlet BC, thin solid line) resulted in a large discrepancy with observed data.

to tidal forcing only, which occurs if there is a hydrologic divide between beach hydraulics and the regional water table. An example was given by Wise et al. (1994) for Kittiwake beach in Alaska. A Dirichlet boundary condition should be used if the landward water table is affected by the regional water table (Mao et al., 2006a; Li and Boufadel, 2010). In the base case, we viewed the water level at PT1 to be only due to tidal forcing, because only the tide was controlled in the experiments of Boufadel et al. (2006). Boufadel (2000) controlled also the water level at PT1 which was used for the purpose of testing a Dirichlet boundary condition. Here we investigate the effect of treating PT1 as a Dirichlet boundary condition for the beach. For this purpose, the observed PT1 values were assigned at the landward boundary in the model and the open water between the screen and left wall was modeled to be only 1.0 cm long in the seaward–andward direction. Considering its assigned high hydraulic conductivity, the 1.0 cm distance ensured that any changes of the water level at PT1 are transmitted almost instantly to the beach.

Fig. 8 shows that the difference between the simulated and observed concentrations using a Dirichlet boundary condition was consistently larger than that obtained using a Neumann boundary condition. The concentration contours under the Dirichlet boundary condition are shown in Fig. 9. In this case, the simulated plume moved more downward and stayed longer in the beach in comparison with the base case (see Fig. 5). The landward extended tail of the plume existed all the time and the freshwater pool close to surface

was smaller than the base case. The movement of the plume might seem counter-intuitive as one expects that the plume moves less downward and more seaward when a Dirichlet boundary condition is used at the landward boundary (PT1). However, for the Dirichlet boundary condition, the observed water table during low tides was much lower than that under Neumann boundary condition, while it was much higher during high tides. This is because a Dirichlet boundary condition constrains the dependent variable (pressure) itself, whereas the Neumann boundary condition constrains the gradient of the pressure, providing higher degrees of freedom to the pressure, and subsequently the water table. The Neumann boundary condition is the equivalent of an integration where the result would be correct to within an arbitrary constant, hence, the higher degree of freedom for Neumann boundary condition. As a consequence for the Dirichlet boundary condition, the seaward hydraulic gradient during low tides was smaller than that under Neumann boundary condition. During high tides, when a Dirichlet boundary condition is applied at PT1, the landward water level rose independently of the tide, and therefore resulted in a downward gradient of the plume. A more detailed investigation of this is left for future work.

To further evaluate the effects of the Dirichlet boundary condition, we computed the mass of applied tracer remaining in the intertidal zone (x from 0.5 m to 4.5 m, Fig. 1) at 10 cm depth. Such information is needed, for example to evaluate the residence time of nutrients for the bioremediation of oil spills on beaches (Wrenn et al., 1997; Li et al., 2007). As shown in Fig. 10a, the mass retained in that zone was always lower under Dirichlet boundary condition than under Neumann boundary condition (base case). This demonstrates that the simulated plume moved more downward and stayed longer in the beach in comparison with the base case.

5.2. Seepage face

A simulation was conducted where the development of the seepage face was suppressed (thus, the water table directly connects to the seawater level). Fig. 10a shows that when the seepage face is not allowed to develop, the mass in the intertidal zone was slightly higher than that in the base case. However, our additional computations show that there is no effect on the overall mass in the beach when the seepage face is neglected (not shown here). As shown in Fig. 10a, the mass under different cases was approaching to a same constant after $t = 9.5$ h.

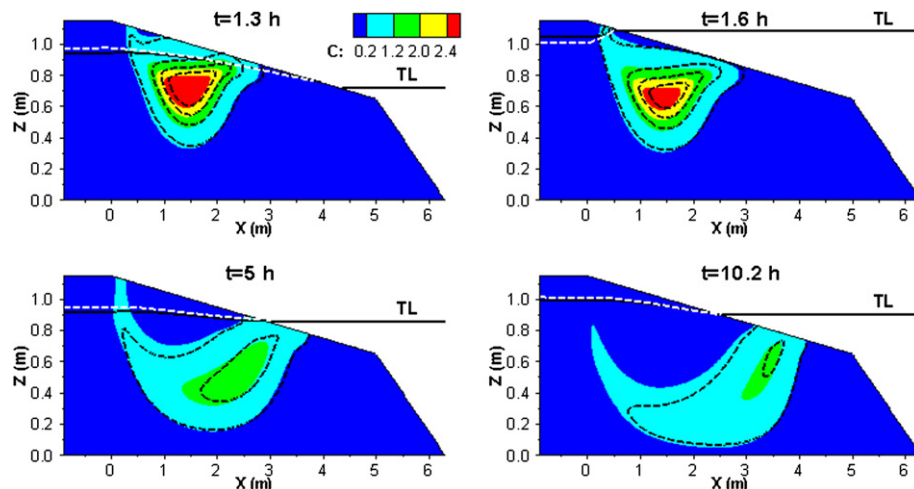


Fig. 9. Concentration (in g/L) contours at different times under the Dirichlet boundary condition along with the base case (dashed lines). Water table under the base case is shown with white dashed line, while water table under the Dirichlet boundary condition is shown with black solid line. The plume moved more downward and stayed longer in the beach in comparison with the base case (Fig. 5).

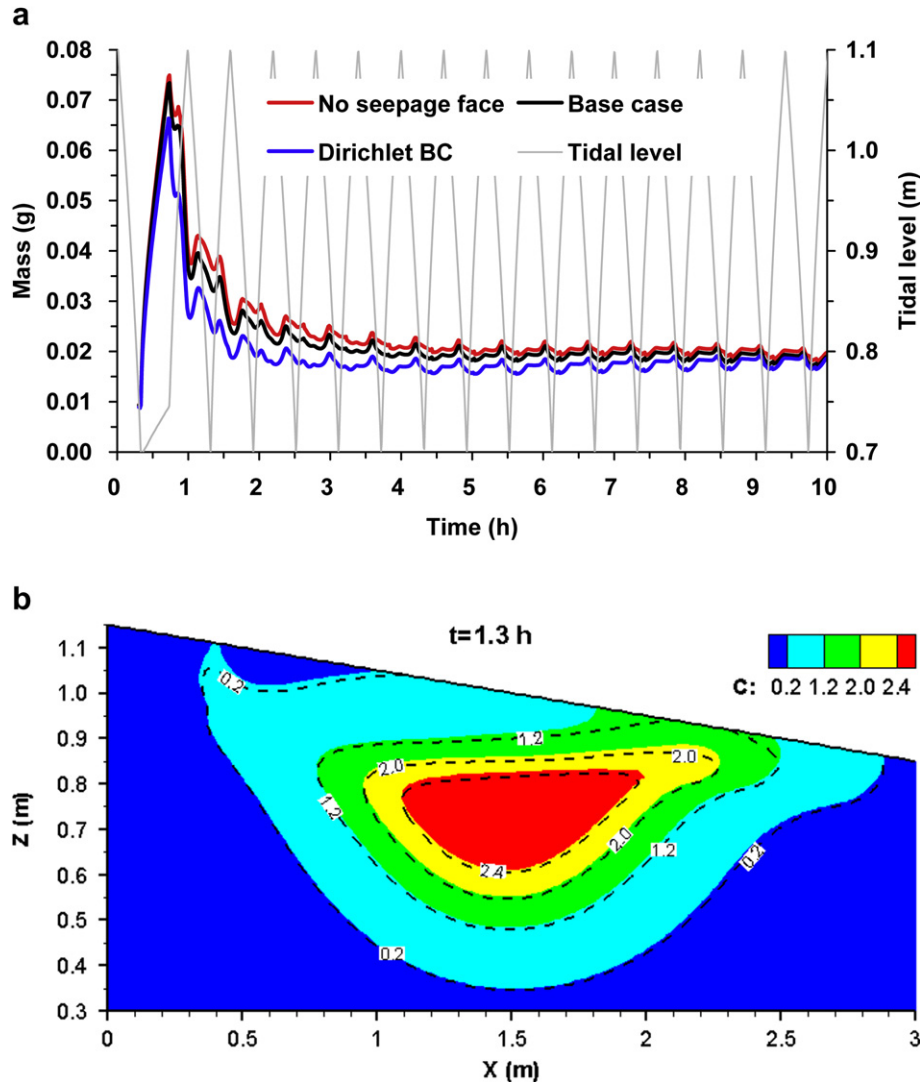


Fig. 10. (a) Change of cumulative masses remaining in the intertidal zone of 10 cm depth with time under the base case, Dirichlet boundary condition and no seepage face case; (b) Concentration (in g/L) distributions at $t = 1.3$ h under the condition of no seepage face (contours) along with the base case (dashed lines), note that excluding seepage face only affects the plume in the shallow part of the beach (~ 10 cm below the beach surface).

Fig. 10b shows that the distribution of the plume at $t = 1.3$ h only has difference in the shallow part (~ 10 cm) of the beach between the base case and the condition of no seepage face, in other word, the concentration in the shallow part was higher without seepage face than the base case. The distribution of the plume at other times had a similar variation but with a smaller difference (not shown in this paper). Thus, neglecting the seepage face would result in an erroneous solute distribution only within the shallow part of the beach, i.e., the location where the seepage flow leaves the beach. However, neglecting the seepage face does not seem to affect the overall movement of solutes in the beach. This could be due to the small slope of the beach (10%), and in that case, neglecting the seepage face did not affect much the location of the water table. Note that the calculated seepage face during the application period reached a length of 1.4 m, and it reached a maximum of 0.6 m afterwards.

5.3. Capillarity

Our previous works (Boufadel, 2000; Naba et al., 2002) indicated that the van Genuchten parameter α (capillarity parameter)

plays a major role in beach dynamics in comparison with “ n ”. Fig. 11 shows the effects of α values on solute concentrations at CM6, CM7, and CM10. Fig. 12 depicts the concentration contours when $\alpha = 10 \text{ m}^{-1}$. Decreasing α value from 25 m^{-1} to 10 m^{-1} resulted in a slow decrease of concentrations with time (Fig. 11), indicating that the tracer plume stayed longer in the beach (Fig. 12). Smaller α value reflect a higher moisture content above the water table which would result in a higher retention of solute in the unsaturated zone (see $t = 44$ min and $t = 1.3$ h). Subsequently, the solute retained above the water table would act as a continuous source of solute to the saturated portion of the beach, which provides a possible reason for the small decreasing rate of the concentration. This speculation was also supported by the higher concentration at CM6 during the whole simulation period when decreasing α value (Fig. 11). Increasing α value (40 m^{-1}) affected the concentration at CM7 and CM10, but significantly affected CM6. However, the effects of increasing α was smaller than that of decreasing it, which is probably due to the fact that the capillary fringe associated with $\alpha = 25 \text{ m}^{-1}$ was already small ($1/\alpha = 0.04 \text{ m}$) and decreasing the capillary fringe to 0.025 m (for $\alpha = 40 \text{ m}^{-1}$) did not make a large difference. Overall, Fig. 11 clearly shows that the effects of the

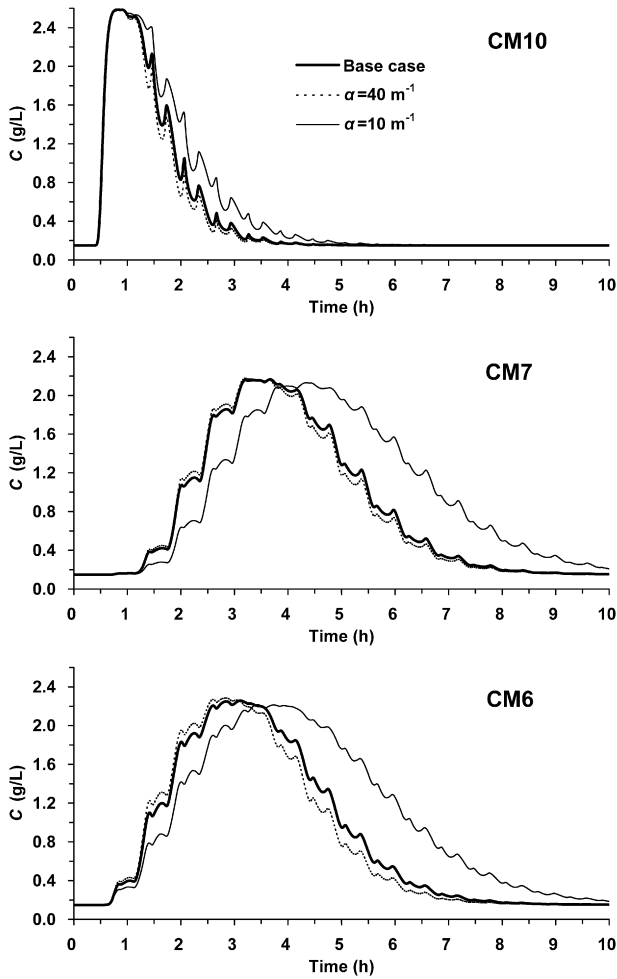


Fig. 11. Changes of the concentrations at CM6, CM7 and CM10 with different α values. Note the depth order: CM6 > CM7 > CM10.

capillarity parameter α on solute concentration increased with depth (CM10 \rightarrow CM7 \rightarrow CM6). Therefore, neglecting capillarity effects has severe consequences on the movement of solutes deep into beaches.

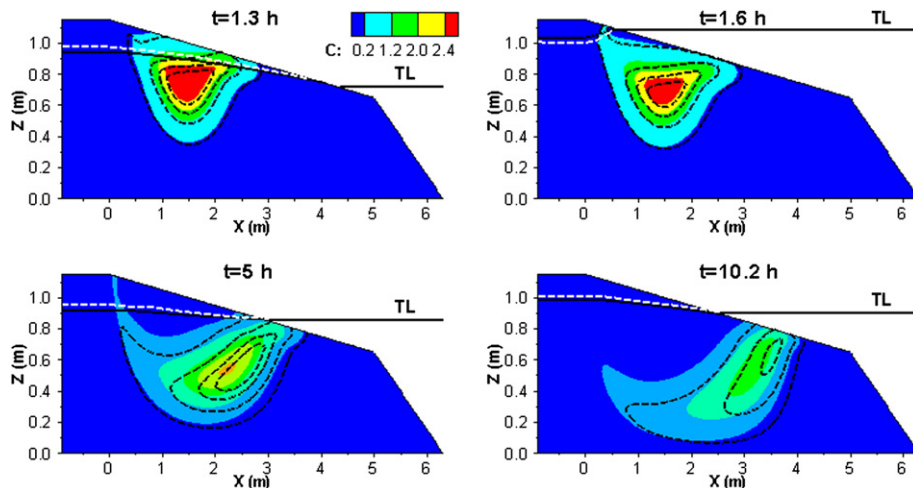


Fig. 12. Concentration (in g/L) contours at different times when $\alpha = 10 \text{ m}^{-1}$ along with the base case (dashed lines). Water table under the base case is shown with white dashed line, while water table when $\alpha = 10 \text{ m}^{-1}$ is shown with black solid line.

Fig. 12 shows that the landward extended tail of the plume existed all the time and was longer (e.g., $t = 5 \text{ h}$) when $\alpha = 10 \text{ m}^{-1}$ than the base case, and thus the freshwater pool close to surface was smaller. Fig. 12 also shows that the water table responded to tide faster in this case than in the base case. Thus capillarity has significant effects on water table and solute transport, and one needs to use a variably saturated model such as SUTRA (Voss and Provost, 2003) or MARUN (Boufadel et al., 1999) when modeling the hydrodynamics of a beach subjected to tide. The exception is for highly coarse beaches where the capillary fringe is negligible. With that in mind, one needs to interpret carefully the simulated results of tidally influenced beaches when using saturated flow models.

5.4. Dispersivity

To investigate the effects of the dispersivity on solute concentration, we conducted four simulations in which α_L value or the ratio α_T/α_L was changed from the base case ($\alpha_L = 2 \text{ cm}$, $\alpha_T/\alpha_L = 0.1$). Fig. 13 shows that increasing α_L values or the ratio α_T/α_L decreased the maximum of the concentration at CM6 compared to the base case, while the maximum of the concentration increased when decreasing α_L values or the ratio α_T/α_L . Fig. 13a shows that the difference with the base case between the simulated results when increasing α_L to 3.0 cm or decreasing it to 1.0 cm while keeping the dispersivity ratio constant is essentially equal. However, Fig. 13b shows that increasing the transverse dispersivity to 0.5 cm created a larger difference with the base case in comparison with decreasing the transverse dispersivity to 0.1 cm. Changing the dispersivity had not effect on the arrival time of the peak at any location, its effects were only limited to the magnitude of the concentration.

6. Generalization of the results

The previous results can be generalized to other situations using the dimensionless formulation of Boufadel et al. (1998) and Boufadel (2000). The approach consists of conducting the following nondimensionalization:

$$\begin{aligned} x^* &= \frac{x}{L_x}, z^* = \frac{z}{L_z}, t^* = \frac{t}{T_0}, T_0 = \frac{L_z}{K_0}, \psi^* = \frac{\psi}{L_z}, \alpha^* = \alpha L_z, \\ \alpha_T^* &= \frac{\alpha_L}{L_x}, \alpha_T^* = \frac{\alpha_T}{L_z} \end{aligned} \quad (12)$$

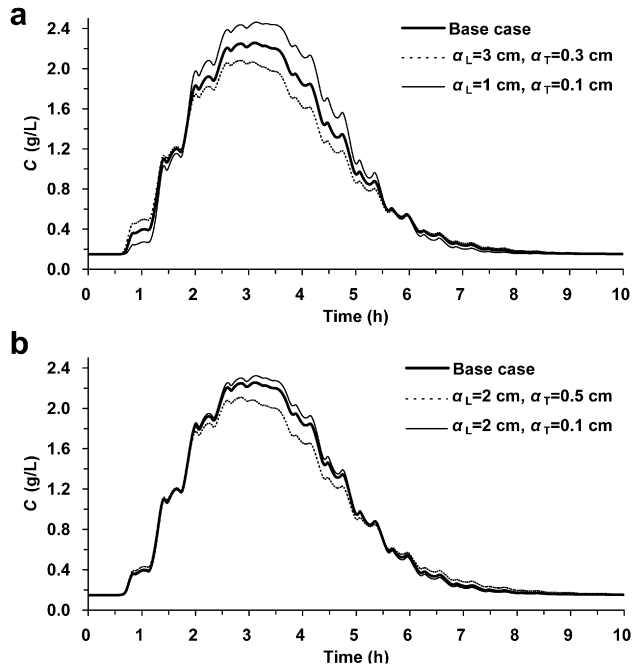


Fig. 13. Changes of the concentration at CM6: (a) with changing the longitudinal dispersivity (α_L) values and (b) with changing the ratio α_T/α_L .

where starred quantities are dimensionless, L_x and L_z are vertical and horizontal dimensions of the beach, respectively. Anisotropy in beaches could be due to alternating microscopic layers of fine and coarse sand (Waddell, 1976), thus a parameter (M) was defined to combine the aspect ratio with the anisotropy ratio:

$$M = \frac{K_{x0}}{K_{z0}} \left(\frac{L_z}{L_x} \right)^2 \quad (13)$$

Other important parameters to conserve are the dimensionless capillary fringe (CF^*)

$$CF^* = \frac{CF}{L_z} \quad (14)$$

In this equation, we are considering, following Boufadel et al. (1999) and Naba et al. (2002) that $CF = 1/\alpha$. The dimensionless tidal period (T^*) is given by:

$$T^* = \frac{T}{\frac{L_z}{K_{z0}}} \quad (15)$$

If a Neumann boundary condition is present (such as in the experiment in this paper), the flow rate in the laboratory model can be written as:

$$F_m = \frac{(K_{z0}L_x)_m F_n}{(K_{z0}L_x)_n} \quad (16)$$

where F_n is the Neumann flow rate in the natural beach, F_m is the Neumann flow rate in the laboratory model, n and m stand for “natural beach” and “laboratory model”.

6.1. Example

The beach in this study could represent a natural beach whose tidal period is 12.25 h with tidal range of 2.0 m. Table 3 lists the properties of a natural beach that could be simulated in the laboratory setup with the sand properties of the base case in this paper. Thus, to generalize the results one proceeds as follows.

- (1) Compute M from the natural beach using equation (13), $M = 0.02$;
- (2) Compute $CF^* = CF/L_z$ from the natural beach whose $CF = 10$ cm and $L_z = 500$ cm. This gives $CF^* = 0.02$, then using it along with the vertical dimension of laboratory beach (115 cm), one can obtain the value of CF for the laboratory beach using equation (14), which gives $CF = 2.3$ cm. Based on this part, one could select the soil that has the CF closest to 2.3 cm (commonly using capillary retention experiments)
- (3) Once the appropriate soil is found, compute the saturated hydraulic conductivity (K_{z0}) using an appropriate method for the expected range of K_0 (Cedergren, 1967, p. 35). Here assume that $K_{z0} = 0.12$ cm/s. Note that the value of K_0 is not important by itself but to scale the tidal period.
- (4) Compute the dimensional tidal period (T^*) of the natural beach using Eq. (15), i.e., $T^* = 12.25 \times 3600 \times 0.01/500 = 0.882$. Then one can find the tidal period for the laboratory beach (based on $K_{z0} = 0.12$ cm/s), $T = 14$ min.
- (5) The tidal amplitude (A) for laboratory beach can be obtained from that of natural beach multiplying by the ratio of L_z for the laboratory beach to that for the natural beach, i.e., $A = 100 \times 115/500 = 23$ cm.
- (6) The Neumann flow rate in our experiment was 0.213 cm²/s, one can obtain the Neumann flow rate in the natural beach using Eq. (16), i.e., $F_n = 0.14$ cm²/s.
- (7) The scaling of the dispersivities is more complicated and we advise the reader to consult the works of Boufadel (2000) for a detailed discussion. Briefly, if the beaches are not too heterogeneous, then one can simply scale up by multiplying by the scale ratio. Thus the natural beach dispersivities are given by:

$$\alpha_L = \frac{0.013}{115} \times 5000 = 0.6 \text{ cm}, \quad \alpha_T = \frac{0.0013}{115} \times 5000 = 0.06 \text{ cm}$$

These values are smaller than commonly observed values which are on the order of a tens of centimeters for α_L and on the order of a centimeter for α_T . If the process is dominated by advection, the error would be small. Otherwise, one would need to increase the natural beach dispersivities obtained by this procedure.

By the above procedure no restriction was put on the value of the saturated hydraulic conductivity (namely K_{z0}), which indicates that it can take any value provided that the unsaturated characteristics (α , n) of soil were selected according to Eq. (14). Note that unless taking extreme values, S_r and ϕ of sandy beaches should not considerably affect water flow (Boufadel et al., 1998; Boufadel, 2000). Thus the generation of the present results using above dimensionless processes is flexible, implying a wide application of the results of the laboratory beach model. The dimensionless formulation allows faithful reproduction of water flow and

Table 3
Design parameters for generalization of the base case.

Parameter	Natural beach	Base case in present paper
L_x (cm)	5000	630
L_z (cm)	500	115
K_{x0} (cm/s)	0.02	0.12
K_{z0} (cm/s)	0.01	0.12
$1/\alpha$ (cm)	10	2.3
α_L (cm)	0.6	0.013
α_T (cm)	0.06	0.0013
Tidal period T	12.25 h	14 min
Tidal amplitude A , cm	100	23
ϕ	0.33	0.33
n	3.5	3.5
S_r	0.01	0.01

advective processes, and might not perform well for dispersion dominated systems. However, it is the only formulation that allows generalization of variably saturated flow results.

7. Conclusions

This paper explored numerical techniques to simulate the movement of an applied tracer plume in a laboratory beach subjected to tide. The MARUN (Boufadel et al., 1999) was used. It is a finite element code that simulates the movement of water in variably saturated porous media while accounting for the effect on solute concentration on water density. As the solute concentration was small in this work, the tracer concentration had no effects on water flow.

The movement of the tracer plume in the beach and the development of a transient seepage on the beach surface were modeled. It was noted that the maximum value of the landward water table was greatly dependent on the time step. Thus, one needs to use a small enough time step (e.g., $\Delta t = 5$ s in this paper) to capture the propagation of the maximum elevation due to tide. By calibrating the results of the numerical model against the observed data, the laboratory beach was found to have two different zones: a top layer (thickness 9–17 cm) with a hydraulic conductivity of 0.2 cm/s and a lower layer with a hydraulic conductivity of 0.12 cm/s. The simulations revealed that the plume moved seaward during falling tides and downward during rising tides, which was consistent with previous studies (e.g., Li et al., 2007). It was also observed that the plume developed a tail that extended in the landward direction, and a freshwater pool became entrapped between the main plume and its extended tail.

A sensitivity analysis was conducted to evaluate the effects of boundary conditions, seepage face development, capillarity, and dispersivity values. It was found that a Dirichlet boundary condition landward of the beach causes the plume of applied tracer to sink deeper into the beach in comparison with a Neumann boundary condition. It also resulted in faster washout of the tracer from the upper part of the beach. The suppression of the seepage face by forcing the water table to match the tide level did not have great effects beach hydrodynamics or on the movement of the tracer, which is probably due to the small slope of the beach (10%). However, seepage flow was around half of the seaward flow leaving the beach through the submerged face. Investigation on the capillarity, through the van Genuchten parameter α revealed that a decrease in the pore size of the beach greatly affects solute hydrodynamics; we noted that the effects on solute transport increase with depth (see Fig. 11). This is probably because a smaller α value results in a higher moisture content above the water table, which allows more of the applied solutes to be retained in the unsaturated zone. The latter would act as a continuous source of solute to the saturated portion of the beach. Thus, we conclude that using a saturated flow model for tidally influenced beaches should be discouraged, especially for fine textured media (i.e., small α or strong capillarity). The simulations also showed that dispersivity does not affect the arriving time of the peak of solute concentration at a specific location but affects its magnitude.

Acknowledgments

This work was supported in part by the grant from the Exxon Valdez Oil Spill Trustee Council under Project (No. 070836). However, it does not necessarily reflect the views of the trustee, and no official endorsement should be inferred.

References

Abdollahi-Nasab, A., Boufadel, M.C., Li, H.L., Weaver, J.W., 2010. Saltwater flushing by freshwater in a laboratory beach. *Journal of Hydrology* 386 (1–4), 1–12.

- Ataie-Ashtiani, B., Volker, R.E., Lockington, D.A., 1999a. Numerical and experimental study of seepage in unconfined aquifers with a periodic boundary condition. *Journal of Hydrology* 222 (1–4), 165–184.
- Ataie-Ashtiani, B., Volker, R.E., Lockington, D.A., 1999b. Tidal effects on sea water intrusion in unconfined aquifers. *Journal of Hydrology* 216 (1–2), 17–31.
- Baird, A.J., Mason, T., Horn, D.P., 1998. Validation of a Boussinesq model of beach ground water behaviour. *Marine Geology* 148, 55–69.
- Bear, J., 1972. *Dynamics of Fluids in Porous Media*. American Elsevier, New York, NY.
- Boufadel, M.C., 2000. A mechanistic study of nonlinear solute transport in a groundwater–surface water system under steady state and transient hydraulic conditions. *Water Resources Research* 36 (9), 2549–2565.
- Boufadel, M.C., Suidan, M.T., Venosa, A.D., 1999. A numerical model for density-and-viscosity-dependent flows in two-dimensional variably saturated porous media. *Journal of Contaminant Hydrology* 37 (1–2), 1–20.
- Boufadel, M.C., Suidan, M.T., Venosa, A.D., 2006. Tracer studies in laboratory beach simulating tidal influences. *Journal of Environmental Engineering* 132 (6), 616–623.
- Boufadel, M.C., Suidan, M.T., Venosa, A.D., Rauch, C.H., Biswas, P., 1998. 2D variably saturated flow: physical scaling and Bayesian estimation. *Journal of Hydrologic Engineering* 3 (4), 223–231.
- Brovelii, A., Mao, X., Barry, D.A., 2007. Numerical modeling of tidal influence on density-dependent contaminant transport. *Water Resources Research* 43 (10), W10426. doi:10.1029/2006WR005173.
- Carrera, J., Neuman, S.P., 1986a. Estimation of aquifer parameters under transient and steady state conditions: 1. Maximum likelihood method incorporating prior information. *Water Resources Research* 22 (2), 199–210.
- Carrera, J., Neuman, S.P., 1986b. Estimation of aquifer parameters under transient and steady state conditions: 2. Uniqueness, stability, and solution algorithms. *Water Resources Research* 22 (2), 211–227.
- Cedergren, H.R., 1967. *Seepage, Drainage, and Flow Nets*. John Wiley & Sons, Inc., New York, NY.
- Cooley, R.L., 1983. Some new procedures for numerical solution of variably saturated flow problems. *Water Resources Research* 19 (5), 1271–1285.
- Destouni, G., Prieto, C., 2003. On the possibility for generic modeling of submarine groundwater discharge. *Biogeochemistry* 66 (1–2), 171–186.
- Frind, E.O., 1982. Simulation of long-term transient density-dependent transport in groundwater. *Advances in Water Resources* 5 (2), 73–88.
- Galeati, G., Gambolati, G., Neuman, S.P., 1992. Coupled and partially coupled Eulerian-Lagrangian model of freshwater-seawater mixing. *Water Resources Research* 28 (1), 149–165.
- van Genuchten, M.T., 1980. A closed-form equation for predicting the hydraulic conductivity of unsaturated soils. *Soil Science Society of America Journal* 44 (5), 892–898.
- Huyakorn, P.S., Andersen, P.F., Mercer, J.W., White, H.O., 1987. Saltwater intrusion in aquifers: development and testing of a three-dimensional finite element model. *Water Resources Research* 23 (2), 293–312.
- Kim, S.-B., Jo, K.-H., Kim, D.-J., Jury, W.A., 2004. Determination of two-dimensional laboratory-scale dispersivities. *Hydrological Processes* 18 (13), 2475–2483.
- Langevin, C.D., Guo, W., 2006. MODFLOW/MT3DMS-based simulation of variable-density ground water flow and transport. *Ground Water* 44 (3), 339–351.
- Li, H.L., Boufadel, M.C., 2010. Long-term persistence of oil from the Exxon Valdez spill in two-layer beaches. *Nature Geoscience* 3, 96–99. doi:10.1038/ngeo749.
- Li, H.L., Boufadel, M.C., Weaver, J.W., 2008. Tide-induced seawater–groundwater circulation in shallow beach aquifers. *Journal of Hydrology* 352 (1–2), 211–224.
- Li, H.L., Zhao, Q.H., Boufadel, M.C., Venosa, A.D., 2007. A universal nutrient application strategy for the bioremediation of oil-polluted beaches. *Marine Pollution Bulletin* 54 (8), 1146–1161.
- Li, L., Barry, D.A., Pattiaratchi, C.B., 1997. Numerical modelling of tide-induced beach water table fluctuations. *Coastal Engineering* 30 (1–2), 105–123.
- Li, L., Barry, D.A., Stagnitti, F., Parlange, J.Y., 1999. Submarine groundwater discharge and associated chemical input to a coastal sea. *Water Resources Research* 35 (11), 3253–3259.
- Mao, X., Enot, P., Barry, D.A., Li, L., Binley, A., Jeng, D.S., 2006a. Tidal influence on behaviour of a coastal aquifer adjacent to a low-relief estuary. *Journal of Hydrology* 327 (1–2), 110–127.
- Mao, X., Prommer, H., Barry, D.A., Langevin, C.D., Panteleit, B., Li, L., 2006b. Three-dimensional model for multi-component reactive transport with variable density groundwater flow. *Environmental Modelling & Software* 21 (5), 615–628.
- Mualem, Y., 1976. A new model for predicting the hydraulic conductivity of unsaturated porous media. *Water Resources Research* 12 (3), 513–522. doi:10.1029/WR012i003p00513.
- Naba, B., Boufadel, M.C., Weaver, J., 2002. The role of capillary forces in steady-state and transient seepage flows. *Ground Water* 40 (4), 407–415.
- Neuman, S.P., 1973. Saturated-unsaturated seepage by finite elements. *Journal of Hydraulics Division, ASCE* 99 (12), 2233–2250.
- Nielsen, P., 1990. Tidal dynamics of the water table in beaches. *Water Resources Research* 26 (9), 2127–2134.
- Park, C.H., Aral, M.M., 2008. Saltwater intrusion hydrodynamics in a tidal aquifer. *Journal of Hydrologic Engineering* 13 (9), 863–872.
- Pinder, G.F., Cooper Jr., H.H., 1970. A numerical technique for calculating the transient position of the saltwater front. *Water Resources Research* 6 (3), 875–882.
- Pinder, G.F., Gray, W.G., 1977. *Finite Element Simulation in Surface and Subsurface Hydrology*. Academic Press, New York, NY, 294 pp.

- Robinson, C., Brovelli, A., Barry, D.A., Li, L., 2009. Tidal influence on BTEX biodegradation in sandy coastal aquifers. *Advances in Water Resources* 32 (1), 16–28.
- Robinson, C., Gibbes, B., Carey, H., Li, L., 2007. Salt-freshwater dynamics in a subterranean estuary over a spring-neap tidal cycle. *Journal of Geophysical Research-Oceans* 112 (C9), C09007. doi:10.1029/2006JC003888.
- Shamir, U., Dagan, G., 1971. Motion of the seawater interface in coastal aquifers: a numerical solution. *Water Resources Research* 7 (3), 644–657.
- Turner, I.L., Coates, B.P., Acworth, R.L., 1997. Tides, waves and the super-elevation of groundwater at the coast. *Journal of Coastal Research* 13 (1), 46–60.
- Venosa, A.D., Suidan, M.T., Wrenn, B.A., Strohmeier, K.L., Haines, J., Eberhart, B.L., King, D., Holder, E., 1996. Bioremediation of an experimental oil spill on the shoreline of Delaware Bay. *Environmental Science and Technology* 30, 1764–1775.
- Voss, C.I., 1984. SUTRA: a Finite-element Model for Saturated–Unsaturated Fluid-Density-Dependent Ground-water Flow with Energy Transport or Chemically Reactive Single-species Solute Transport. USGS Water-Resources Investigations Report 84-4369, USGS. US Geological Survey, Reston, VA.
- Voss, C.I., Provost, A.M., 2003. SUTRA: a Model for Saturated–Unsaturated, Variable-Density Ground-Water Flow with Solute or Energy Transport. US Geological Survey Water-Resources Investigations Report 02–4231. US Geological Survey, Reston, Virginia.
- Waddell, E., 1976. Swash–groundwater–beach profile interactions. In: *SEPM Special Publications*, vol. 24, pp. 115–125.
- Wise, W.R., Clement, T.P., Molz, F.J., 1994. Variably saturated modeling of transient drainage: sensitivity to soil properties. *Journal of Hydrology* 161 (1–4), 91–108.
- Wrenn, B.A., Suidan, M.T., Strohmeier, K.L., Eberhart, B.L., Wilson, G.J., Venosa, A.D., 1997. Nutrient transport during bioremediation of contaminated beaches: evaluation with lithium as a conservative tracer. *Water Research* 31 (3), 515–524.
- Xia, Y.Q., Li, H.L., Boufadel, M.C., Sharifi, Y., 2010. Hydrodynamic factors affecting the persistence of the Exxon Valdez oil in a shallow bedrock beach. *Water Resources Research* 46, W10528. doi:10.1029/2010WR009179.
- Yeh, G.T., 1981. On the computation of Darcian velocity and mass balance in the finite element modeling of groundwater flow. *Water Resources Research* 17 (5), 1529–1534.
- Zhang, Q., Volker, R.E., Lockington, D.A., 2001. Influence of seaward boundary condition on contaminant transport in unconfined coastal aquifers. *Journal of Contaminant Hydrology* 49 (3–4), 201–215.
- Zhang, Q., Volker, R.E., Lockington, D.A., 2002. Experimental investigation of contaminant transport in coastal groundwater. *Advances in Environmental Research* 6 (3), 229–237.